Spectroscopic determination of magnetic-field-dependent interactions in an ultracold Yb(^{3}P)-Li mixture

AUTHOR(S):

Schäfer, Florian; Konishi, Hideki; Bouscal, Adrien; Yagami, Tomoya; Takahashi, Yoshiro

CITATION:

Schäfer, Florian ...[et al]. Spectroscopic determination of magnetic-field-dependent interactions in an ultracold Yb(^{3}P)-Li mixture. Physical Review A 2017, 96(3): 032711.

ISSUE DATE:

2017-09

URL:

http://hdl.handle.net/2433/244801

PHYSICAL REVIEW A **96**, 032711 (2017)

Spectroscopic determination of magnetic-field-dependent interactions in an ultracold Yb($^3P_2$)-Li mixture

F. Schäfer,[1,*] H. Konishi,[1] A. Bouscal,[1,2] T. Yagami,[1] and Y. Takahashi[1]
[1]*Department of Physics, Graduate School of Science, Kyoto University, Kyoto 606-8502, Japan*
[2]*Department of Physics, École Normale Supérieure, 24 Rue Lhomond, F-75231 Paris Cedex 05, France*
(Received 31 July 2017; published 18 September 2017)

We present experimental results on the inelastic and elastic interspecies interactions between ytterbium (Yb) in the metastable $^3P_2$ state loaded into a deep optical lattice and spin polarized lithium (Li) in its ground state. Focusing on the $m_J = 0$ magnetic sublevel of Yb($^3P_2$), bias magnetic fields between 20 and 800 G are investigated and significantly enhanced inelastic collision rates with high magnetic fields are found. In addition, by direct spectroscopy of the Yb Mott insulator immersed in the Li Fermi gas an upper boundary of the background scattering length of the Yb($^3P_2, m_J = 0$)-Li($^2S_{1/2}, F = 1/2, m_F = +1/2$) system is estimated, revealing the absence of useful Feshbach resonances. These observations are qualitatively consistent with the theoretical calculations.

DOI: 10.1103/PhysRevA.96.032711

I. INTRODUCTION

Experiments in ultracold quantum degenerate gases have proven to be an invaluable asset in the study of quantum phenomena [1,2]. Especially the defect-free preparation of samples in optical lattices [3] allowed for unprecedented control in realizing the Bose-Hubbard model [4] and is seen as a promising platform to realize topological matter [5]. Success is facilitated by an unparalleled controllability of the particle interactions by means of magnetically tunable Feshbach resonances [6]. In recent years multicomponent quantum gases also came into focus [7] with applications in quantum simulation of impurity systems [8] and in the production of ultracold molecules [9,10]. Large progress was made in the formation of ground-state alkali-metal dimers [11], and their applications to ultracold chemistry [12] and dipolar collisional physics [13] were reported.

Shifting away from alkali-metal dimers to compounds including alkaline-earth or alkaline-earth-metal-like species a new class of molecules with doublet ground states ($^2\Sigma$ molecules) becomes possible. New applications in quantum state preparation [14] and information processing [15] are envisioned. Production approaches include the photoassociation of molecules [11,16], buffer gas loading techniques [17,18], and direct laser cooling [19]. Mandatory to the formation of ultracold $^2\Sigma$ molecules is a good understanding of the interspecies interactions and the control thereof [20]. The possibility of magnetically tunable Feshbach resonances in those systems was confirmed theoretically [21], however, the predicted resonances are very narrow [22]. Later it was discussed that due to anisotropy in the interaction involving the metastable $^3P_2$ state [23] possibly experimentally exploitable, broad magnetic Feshbach resonances are supported by the ytterbium (Yb)-lithium (Li) collisional system, where the alkaline-earth-metal-like Yb is in the metastable $^3P_2$ state [24–26]. At the same time, those theories predict quite large inelastic two-body collisional processes and thus the suppression of a large variation of the scattering lengths around the Feshbach resonances.

Due to the complexity of the calculations involved and insufficient knowledge on the precise interaction potentials, reliable predictions on the Yb($^3P_2$)-Li Feshbach resonance landscape are as of yet missing. Experimentally, a first signature of a Feshbach resonance in ^{174}Yb($^3P_2, m_J = -1$)-^{6}Li($^2S_{1/2}, F = 1/2, m_F = +1/2$) collisions was found [27] leading to improved model calculations [25]. In a different work [28] the inelastic loss coefficient in the energetically lowest state, ^{174}Yb($^3P_2, m_J = -2$)-^{6}Li($^2S_{1/2}, F = 1/2, m_F = +1/2$), at low magnetic bias fields and the involved inelastic loss channels were discussed. Most recently, the importance of anisotropy induced losses and their possible suppression using stretched states was experimentally highlighted [29].

The purpose of the present work is to further broaden our knowledge on the ^{174}Yb($^3P_2$)-^{6}Li($^2S_{1/2}$) collisional system. We experimentally investigate the inelastic losses in collisions of ^{174}Yb($^3P_2, m_J = 0$) with ground-state ^{6}Li in the Zeeman states $F = 1/2$, $m_F = \pm 1/2$ and $F = 3/2$, $m_F = \pm 3/2$ for bias magnetic fields between 20 and 800 G. Further, by direct spectroscopic investigation of the ultranarrow Yb($^1S_0 \rightarrow {}^3P_2$) transition we gain direct access to the elastic part of the interspecies scattering length and estimate an upper bound for it.

This paper is organized as follows. In Sec. II, we review the experimental idea and details on its execution. Section III presents the data and its analysis. In Sec. IV we conclude by a discussion of the results and their significance.

II. EXPERIMENT

The experiment started with a degenerate mixture of bosonic ^{174}Yb and fermionic ^{6}Li as detailed in [29,30]. (In the remainder of the present text we will suppress the atomic mass notation for clarity.) In brief, by combination of optical pumping of Li, forced evaporation of Yb in a far off-resonance optical trap (FORT) and sympathetic cooling of Li by Yb, quantum degenerate gases of typically 10^5 Yb atoms and 3×10^4 spin polarized Li atoms were created and held in a crossed FORT configuration. Li atoms could be prepared with purities >90% in four different Zeeman

*schaefer@scphys.kyoto-u.ac.jp

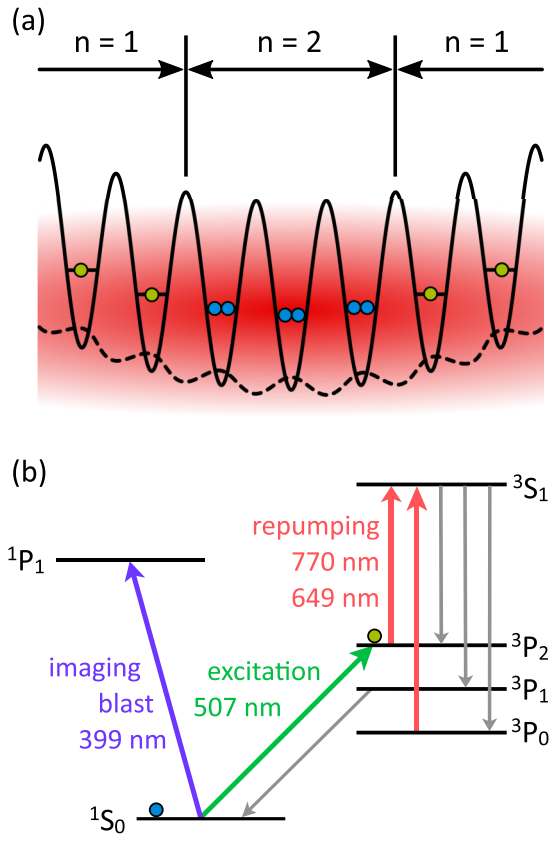

FIG. 1. (a) Quantum degenerate mixture of Yb and Li loaded into a 3D optical lattice. The effective lattice potential for Yb (solid line) is deep at 15 E_R^{Yb} and a Mott-insulator shell structure (blue and green dots) is formed. For clarity only lattice occupation numbers $n = 1$ and 2 are shown. The effective Li potential (dashed line) is with only 0.7 E_R^{Li} shallow and Li unlocalized (red cloud). In the experiment the interactions between Yb($^3P_2$) atoms (green dots) in $n = 1$ sites and Li are investigated. (b) Yb level spectrum of importance to the experiment. The excitation laser (green) connects the ground to the metastable $^3P_2$ state. For imaging purposes (blue) two repumping lasers (red) are used to repopulate the $^1S_0$ state.

states, $F = 1/2, m_F = \pm 1/2$ and $F = 3/2, m_F = \pm 3/2$. The temperature of Li was $T_{\mathrm{Li}} \approx 300$ nK and $T_{\mathrm{Li}}/T_{\mathrm{F}} \approx 0.2$, where T_{F} is the Fermi temperature.

The experimental idea for the precise and magnetic sublevel resolved spectroscopic determination of the Yb($^3P_2$)-Li interactions is sketched in Fig. 1(a). The necessary Yb optical transitions are summarized in Fig. 1(b). Similar to our previous work [29] the Yb atoms were prepared in a Mott-insulating state by adiabatic loading of a three-dimensional optical lattice with lattice constant 266 nm. The lattice depth with respect to Yb($^1S_0$) was $15E_R^{\mathrm{Yb}}$, where E_R denotes the recoil energy, and was for Yb($^3P_2$) due to different polarizabilities a factor 1–1.4 deeper. By virtue of its low mass the lattice depth for Li was only $0.7E_R^{\mathrm{Li}}$ and the Li density distribution was only weakly modulated by the lattice. At the lattice wavelength the polarizability of Li is negative and the lattice sites of Li and Yb alternate. By application of a gravitational sag compensation beam [28] while ramping up the lattice the final separation between the Yb and Li cloud center-of-mass positions could be reduced to (3.5 ± 1.0) μm. Typical atom cloud radii in vertical direction were 3.5 μm for Yb and 4.0 μm for Li, and the remaining center-of-mass difference was accounted for in the data analysis.

For measurements of the interspecies inelastic decay described in detail in Sec. III A only Yb atoms in singly occupied lattice sites ($n = 1$) were selectively transferred into the metastable $^3P_2$ state by a 0.5-ms pulse of 507-nm laser light. The laser frequency was during this time linearly ramped from -4 kHz to $+4$ kHz with respect to the transition resonance frequency in order to improve excitation reproducibility. By virtue of the Yb-Yb intraspecies interaction the resonance frequencies for Yb($^1S_0$) atoms in $n > 1$ sites were shifted by more than 4 kHz and accordingly not excited [31]. Care was taken to choose the light intensity such as to only excite about 2×10^3 to 3×10^3 Yb atoms, corresponding to about 10% of the total number of Li atoms. Sample preparation was completed by removal of remaining Yb($^1S_0$) atoms via a 0.3-ms resonant light pulse at 399 nm. This ensured that due to Yb residual site hoppings a decay of metastable Yb atoms by collisions with Yb($^1S_0$), known to be highly inelastic [32], was excluded.

Two magnetic coils in Helmholtz configuration provide up to 800-G magnetic bias field at the position of the atoms. Magnetic field calibration was done by observation of the narrow Li Feshbach resonance at 543 G [33] and linear extrapolation. Linearity was guaranteed by a temperature stabilized closed-loop feedback system of the coil current. The residual uncertainty in the magnetic fields was estimated to be 0.5% of the nominal value. It was further confirmed that possible effects of magnetic field inhomogeneities on the position of the magnetically sensitive Li atom cloud were smaller than the uncertainty in the final, gravity induced Yb-Li cloud separation. To prevent detrimental effects of a magnetic field ramp on the measurement results it was desirable to set the magnetic field before excitation to the metastable state. We note that in fact we found that a field ramp-up sequence after excitation to the $^3P_2$ state at low magnetic field introduced severe instability of the signals, possibly due to the metastable state already decaying during the field ramp-up process. Due to the strong Zeeman splitting of the metastable Yb state of 2.1 MHz/G$\times m_J$ the constraint of an excitation only at high fields limited the choice of possible Zeeman states to the magnetically insensitive $m_J = 0$ one. At magnetic field strengths beyond about 300 G excitation to the $^3P_2$ state was facilitated by magnetic admixture of the $^3P_1$ state. For low fields and due to experimental constraints in our choice of relative field polarizations efficient excitation was not possible. Therefore we chose to perform for target fields below 300-G excitation to the metastable state at 300 G followed by a fast 0.3-ms ramp (the duration of the 399-nm sample cleaning pulse) down to the target field. In all cases the upwards ramp after loading Yb into the lattice and before excitation to the metastable state was 20 ms in duration.

After sample and magnetic field preparation a variable holding time was followed by a second cleaning pulse at 399 nm. This guaranteed that only the remaining Yb($^3P_2$) atoms were detected after the interaction time by preventing any spontaneous or collision induced Yb($^3P_2 \rightarrow {}^1S_0$) events not leading to trap loss from contaminating the experimental signal. Detection of the remaining atoms was done after

repumping to the $^1S_0$ ground state, Fig. 1(b), by recording the fluorescence light of a detection MOT operating on the strong $^1S_0$-$^1P_1$ transition at 399 nm. The number of Li atoms was simultaneously recorded by standard absorption imaging. Repetition of the complete sequence for interaction times typically between 0 and 30 ms gave access to the necessary decay information.

In a second set of measurements, see Sec. III B, the on-site interaction energy between Li and Yb($^3P_2$) was probed directly by measuring the induced shift of the Yb($^1S_0 \rightarrow {}^3P_2$) transition energy [28]. This required two modifications to the experimental sequence. First, excitation to the metastable state was done with a 0.3-ms pulse of constant frequency. Second, after the first cleaning pulse no further interaction time was necessary and the number of Yb($^3P_2$) atoms was directly recorded by fluorescence imaging. Repeating the modified sequence with excitation frequencies typically ± 10 kHz about the resonance frequency revealed the $n = 1$ excitation spectrum.

In both cases the measurements were completed by taking additional reference data where the cloud of Li atoms was removed from the experiment by application of a strong blasting light resonant to the Li D2 line after completing the forced evaporation and before loading the atoms into the optical lattice. All measurements were repeated five times.

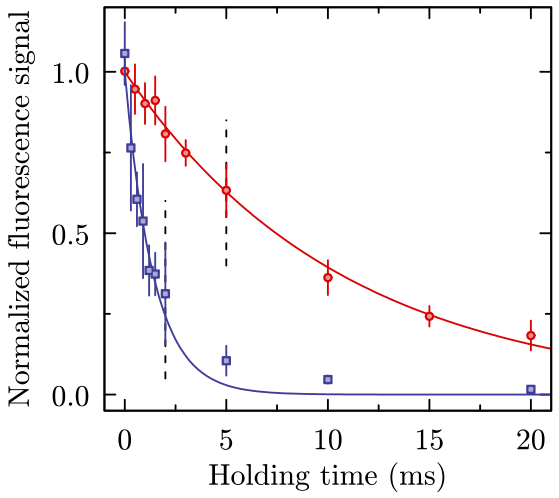

FIG. 2. Experimental decay signal and lifetime determination. For the inelastic Yb($^3P_2, m_J = 0$)-Li($F = 1/2, m_F = +1/2$) collisional process the decay of metastable Yb atoms is shown at magnetic bias field strength of 20 G (red circles) and 600 G (blue squares). Lines indicate exponential fits to the data where data points up to 5 and 2 ms (dashed lines), respectively, were evaluated. Lifetimes were found to be $10.7^{+1.3}_{-0.8}$ ms and $1.4^{+0.2}_{-0.1}$ ms. The error bars indicate the standard deviation over typically five independent executions of the measurement.

III. ANALYSIS AND RESULTS

In the following we show the experimental data obtained and present their analysis. The results concerning the inelastic collisional properties are treated in Sec. III A, those regarding the elastic interactions are elucidated in Sec. III B.

A. Inelastic losses

We measured the magnetic field and spin dependence of the inelastic loss coefficient by observation of the Yb($^3P_2$) decay curve for each of the four accessible Li Zeeman states and magnetic bias fields between 20 and 800 G in steps of 20 G. As an example, the obtained decay signals for the Yb($^3P_2, m_J = 0$)-Li($F = 1/2, m_F = +1/2$) collisional process at 20 and 600 G are reproduced in Fig. 2. A significantly shorter lifetime at 600 G is observed. For the analysis we start with the usual ansatz [28,29] for the density n_{Yb} of Yb atoms in the metastable state,

$$\dot{n}_{\mathrm{Yb}}(\mathbf{r},t) = -\alpha\, n_{\mathrm{Yb}}(\mathbf{r},t) - \beta\, \xi\, n_{\mathrm{Li}}(\mathbf{r})\, n_{\mathrm{Yb}}(\mathbf{r},t). \qquad (1)$$

Here α is the one-body and β the Yb($^3P_2$)-Li inelastic loss rate. The slight reduction of the Li density n_{Li} at the Yb lattice sites due to the optical lattice potential is described by the density correction factor ξ. It is evaluated to $\xi = 0.65 \pm 0.03$ by the overlap integral of the Li Bloch wave function and the Yb Wannier state [28]. The preparation of localized Yb($^3P_2$) atoms in $n = 1$ sites and the removal of remaining Yb($^1S_0$) atoms ensures that collisions with other Yb atoms are negligible. Also, by restricting the number of metastable Yb atoms to about 10% of the total number of Li atoms it is justified to assume n_{Li} as constant during the holding times of interest here. Similarly, the experiment showed no significant change in the temperature of the Li sample. The one-body loss rate α is determined to be $\alpha^{-1} = (850 \pm 300)$ ms by our independent reference measurements in which Li was removed from the sample. As discussed in [29] the inelastic loss rate β can be reliably deduced from the initial exponential decay of the total number of Yb($^3P_2$) atoms N_{Yb}. Assuming for short interaction times,

$$N_{\mathrm{Yb}}(t) = N_{\mathrm{Yb}}(0)\, \exp(-t/\tau_{\mathrm{expt}}), \qquad (2)$$

gives rise to an experimental lifetime τ_{expt}. Comparison of the slope at $t = 0$ of Eq. (2) to the initial decay described by the spatial integral of Eq. (1),

$$\dot{N}_{\mathrm{Yb}}(t=0) = -\alpha\, N_{\mathrm{Yb}}(t=0) - \beta\, \xi \int n_{\mathrm{Li}}(\mathbf{r})\, n_{\mathrm{Yb}}(\mathbf{r},0)\, d^3r, \qquad (3)$$

yields together with the overlap integral $X = \int n_{\mathrm{Li}}(\mathbf{r})\, n_{\mathrm{Yb}}(\mathbf{r},0)\, d^3r$ the inelastic loss rate,

$$\beta = \frac{N_{\mathrm{Yb}}(0)}{\xi\, X}\left(\frac{1}{\tau_{\mathrm{expt}}} - \alpha\right). \qquad (4)$$

During the evaluation of X care is taken to include remnant center-of-mass offsets between the Yb and Li clouds. In the analysis typically the first seven data points, corresponding to holding times up to between 2 and 5 ms, are included for the determination of τ_{expt}; cf. dashed lines in Fig. 2.

In a two-step bootstrap approach the uncertainties in the analysis are evaluated. First, by random resampling and reanalysis of the experimental data a distribution for τ_{expt} is determined. Then, repeated evaluation of Eq. (4) while randomly drawing values from the distribution of τ_{expt} and from assumed ranges of the remaining parameters a distribution for β is obtained. See [29] for a detailed discussion and the value

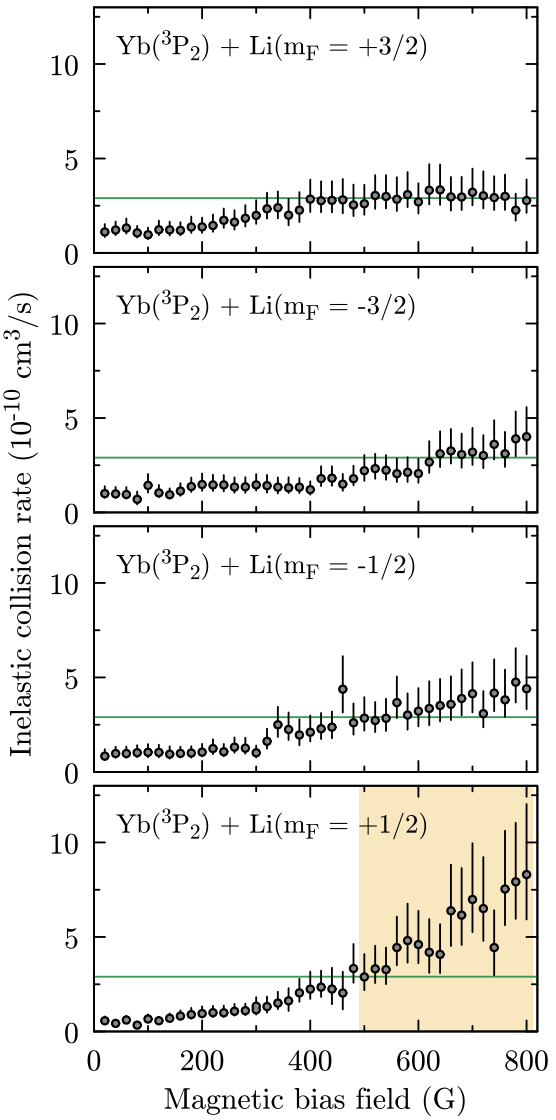

FIG. 3. Survey of inelastic collision rates for Yb($^3P_2, m_J = 0$)-Li($^2S_{1/2}$) collisions in magnetic bias field ranges between 20 and 800 G. The Li sample is prepared in either the $F = 1/2, m_F = \pm 1/2$ state (lower two panels) or the $F = 3/2, m_F = \pm 3/2$ state (upper two panels). All panels are reproduced in the same scale and a smooth increase of the inelastic collision rates is observed in all four cases. No distinct resonance-like features are found that might indicate the presence of an underlying Feshbach resonance. See the main text for a discussion of the error bars. Also shown is the expected universal rate (green lines) and the shaded area (yellow) marks the parameter range in which additionally spectroscopic data on elastic properties was obtained; see Sec. III B.

ranges used also here. The quantiles at 50%, 15.9%, and 84.1% then give the best estimator and a 1-σ confidence interval.

The results for the different Li Zeeman states are shown in Fig. 3. At the lowest magnetic field, 20 G, we observe similarly about 1×10^{-10} cm^3/s in all four cases. This is in good agreement with our earlier results [29] obtained at 0.2 G. For increased magnetic fields up to approximately 400 G only a moderate increase in the inelastic collision rate is observed. Then, up to the highest fields at 800 G, in collisions with Li($F = 1/2, m_F = +1/2$) strongly enhanced losses up to $8^{+4}_{-3}\times10^{-10}$ cm^3/s are found. The same tendency can be seen in the remaining cases, albeit to lesser extents, the inelastic rates staying below 5×10^{-10} cm^3/s. Pronounced peaks in the losses, indicative of possible Feshbach resonances, are not observed.

B. Elastic interspecies interactions

Using interspecies thermalization measurements [30,34] and an analysis of the bosonic dipole oscillation frequency shift in a superfluid Yb-Li mixture [35] the Yb-Li ground-state scattering length is known to be $a_{\mathrm{Yb}(^1S_0)\mathrm{Li}} = (+15 \pm 2)\, a_0$, where a_0 is the Bohr radius. In contrast, the present work probes the interspecies scattering length $a_{\mathrm{Yb}(^3P_2)\mathrm{Li}}$ between metastable Yb and Li. By measuring the frequency spectrum of the Yb($^3P_2$) Mott insulator $n = 1$ shell direct access to on-site interaction energies is gained. By comparison of the resonance positions in the presence and absence of Li a sensitive probe to the interspecies interaction [1],

$$U_{\mathrm{YbLi}} = \frac{2\pi\hbar^2\, a_{\mathrm{YbLi}}}{m_{\mathrm{red}}} \int |w_{\mathrm{Yb}}(\mathbf{r})|^2 |\psi_{\mathrm{Li}}(\mathbf{r})|^2 n_{\mathrm{Li}}(\mathbf{r})\, d^3\mathbf{r}, \quad (5)$$

is obtained. Here, a_{YbLi} is the interspecies scattering length, m_{red} is the reduced mass, and w_{Yb} and ψ_{Li} are the Yb Wannier and Li Bloch wave functions. The integral is taken over the volume of a single lattice site and simplifies to

$$U_{\mathrm{YbLi}} = \frac{2\pi\hbar^2\, a_{\mathrm{YbLi}}}{m_{\mathrm{red}}}\, \xi\, n_{\mathrm{Li}}. \quad (6)$$

Our experimental signal is sensitive to a shift of the spectral line and thus to a change in the interaction energy $U_{\mathrm{Yb}(^3P_2)\mathrm{Li}} - U_{\mathrm{Yb}(^1S_0)\mathrm{Li}}$ as depicted in Fig. 4(a). Assuming typically $n_{\mathrm{Li}} = 3\times10^{12}$ cm^{-3} one finds that a resonance shift of +0.5 kHz corresponds to a change in the scattering length by $a_{\mathrm{Yb}(^3P_2)\mathrm{Li}} - a_{\mathrm{Yb}(^1S_0)\mathrm{Li}} \approx 23$ nm $= 440\, a_0$.

Data was taken for magnetic fields > 500 G where magnetic mixing with the $^3P_1$ state ensured a strong spectroscopic signal. We concentrated on the Yb($^3P_2, m_J = 0$)-Li($^1S_0, F = 1/2, m_F = +1/2$) case where the largest change of the inelastic rate for high fields was observed, see shaded region in Fig. 3. The spectroscopic data at 500 G is shown in Fig. 4(b). The fluorescence signal with Li (blue) generally shows a lower amplitude than the data without it (red). This is due to the partial decay of the Yb($^3P_2$) atoms during excitation (0.3 ms), removal of Yb($^1S_0$) atoms (0.3 ms) and repumping (1 ms). Of importance here, however, is a possible shift of the spectroscopic line. Gaussian fits to the data reveal in this case a frequency up-shift by (0.4 ± 0.2) kHz, corresponding to $a_{\mathrm{Yb}(^3P_2)\mathrm{Li}} - a_{\mathrm{Yb}(^1S_0)\mathrm{Li}} = (350 \pm 180) a_0$. In Fig. 4(c) we summarize the measured frequency shifts up to 800 G. Even though the inelastic rate shows variations by a factor of two in this range the observed frequency shifts remain below 0.5 kHz limiting the change of a_{YbLi} to below $400\, a_0$. Between 620 and 780 G a positive frequency shift of (0.17 ± 0.15) kHz is observed (cf. shaded area in Fig. 4) which corresponds to an increase of the interspecies scattering length by $(150 \pm 130)\, a_0$.

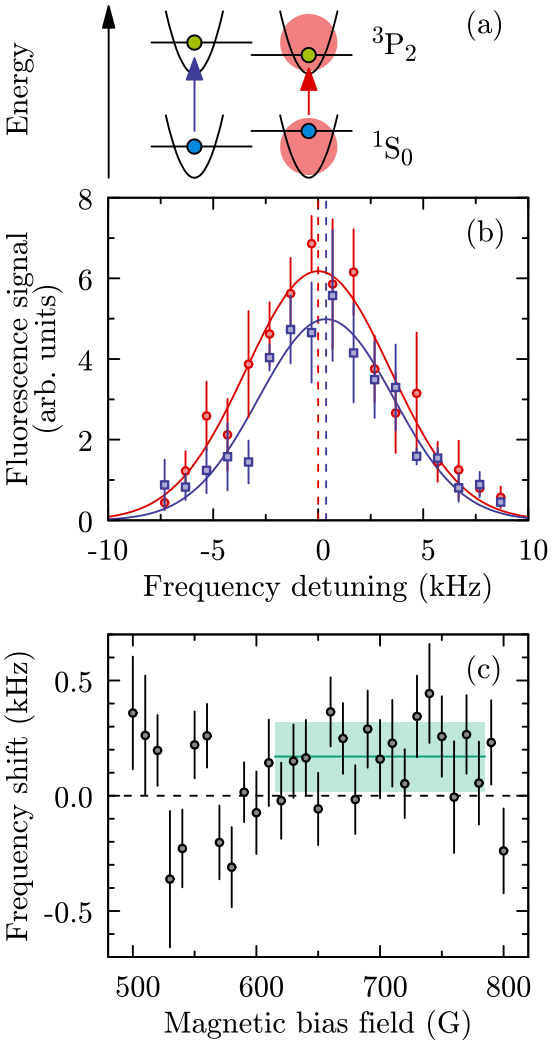

FIG. 4. Direct spectroscopy of Yb($^3P_2$)-Li($F=1/2, m_F=+1/2$) interspecies interaction. (a) Sketch of the measurement principle where a change in the interaction energy between Li (red) and Yb in either $^1S_0$ (blue) or $^3P_2$ (green) state leads to a shift of the transition energy (arrows). (b) Excitation spectra for singly occupied lattice sites at a lattice depth of 15 E_R^{Yb} and at 500 G magnetic bias field. With respect to the reference measurement without Li (red circles) a reduction of the peak height and a slight shift towards higher excitation frequencies in the case with Li (blue squares) is observed. The data are fitted by Gaussian functions (lines). Error bars denote the standard error from five measurements and the frequency detuning is set to zero when in resonance with the reference measurements. (c) Summary of the spectroscopic line shifts obtained in the range 50–800 G. Data were taken in steps of 10 G and the frequency shifts with respect to a corresponding reference measurement without Li obtained by Gaussian fitting are reported here together with the fitting 1-σ error estimates. The dashed line is to mark vanishing frequency shifts. In the range 620–780 G a small positive frequency shift is observed (green line and shaded areas as 1-σ confidence interval).

IV. DISCUSSION AND CONCLUSION

Using high-resolution spectroscopic measurements we analyze both the inelastic collisional rates and the elastic interspecies interactions between Yb($^3P_2, m_J=0$) atoms and four Zeeman states of ground state Li for magnetic field strengths up to 800 G. We find in general moderate inelastic loss rates of about 10^{-10} cm^3/s at low fields. At our highest fields increased rates are found that still remain below 10^{-9} cm^3/s. The increase is generally found to be smooth and picks up strength for fields beyond about 400 G. No resonance-like structures are observed. Focusing on a parameter range with a particular strong change in the inelastic properties we directly investigate the on-site Yb($^3P_2, m_J=0$)-Li($F=1/2, m_F=+1/2$) interaction energy. The observed frequency shifts remain below ± 0.4 kHz. In the theoretical work Ref. [24] generally, even at predicted strong Feshbach resonances, $|a_{\mathrm{Yb}(^3P_2)\mathrm{Li}}| < 1000\, a_0$ is found corresponding to a resonance shift of about 1 kHz. At other magnetic fields scattering lengths remaining below $200\, a_0$ are predicted. In the range between 620 and 780 G a systematic, nonzero shift prevails that indicates a small but finite increase of $a_{\mathrm{Yb}(^3P_2)\mathrm{Li}}$ with respect to $a_{\mathrm{Yb}(^1S_0)\mathrm{Li}}$ by about $150\, a_0$.

The inelastic collision rates reported here are generally higher than those theoretically predicted in [24] for collisions with Yb($^3P_2, m_J=-2$) and go beyond the estimated universal rate [24,36] of 2.9×10^{-10} cm^3/s; cf. green lines in Fig. 3. The observed strong losses highlight the effectiveness of relaxation processes driven by the anisotropic Yb($^3P_2$)-Li interaction potential. The measured on-site Yb($^3P_2$)-Li interaction energy confirms the expected moderate variability [24] of $a_{\mathrm{Yb}(^3P_2)\mathrm{Li}}$. The absence of resonant-like behavior in all our data is striking and should motivate corresponding studies. The survey of parameters presented in the current paper is to serve as a basis for a discussion on the coarse structure of the Yb($^3P_2$)-Li interactions. In the future, experiments with greater resolution might reveal resonance structures with small widths that were beyond the scope of the present research. It will be further theoretically of great interest and experimentally challenging to expand the methods presented here to measurements of the energetically lowest but strongly magnetic-field-dependent $m_J=-2$ substate of Yb($^3P_2$).

ACKNOWLEDGMENTS

The authors would like to thank A. Kell for invaluable help in an early stage of the experiment. This work was supported by the Grant-in-Aid for Scientific Research of JSPS Grants No. JP25220711, No. JP26247064, No. JP16H00990, No. JP16H01053, and No. JP17H06138, JST CREST Grant No. JPMJCR1673, and the Impulsing Paradigm Change through Disruptive Technologies (ImPACT) program by the Cabinet Office, Government of Japan. H.K. acknowledges support from JSPS.

[1] I. Bloch, J. Dalibard, and W. Zwerger, Rev. Mod. Phys. **80**, 885 (2008).

[2] I. Bloch, J. Dalibard, and S. Nascimbène, Nat. Phys. **8**, 267 (2012).

[3] S. Giorgini, L. P. Pitaevskii, and S. Stringari, Rev. Mod. Phys. **80**, 1215 (2008).
[4] I. Bloch, Nat. Phys. **1**, 23 (2005).
[5] N. Goldman, J. C. Budich, and P. Zoller, Nat. Phys. **12**, 639 (2016).
[6] C. Chin, R. Grimm, P. Julienne, and E. Tiesinga, Rev. Mod. Phys. **82**, 1225 (2010).
[7] C. J. Myatt, E. A. Burt, R. W. Ghrist, E. A. Cornell, and C. E. Wieman, Phys. Rev. Lett. **78**, 586 (1997).
[8] P. Massignan, M. Zaccanti, and G. M. Bruun, Rep. Prog. Phys. **77**, 034401 (2014).
[9] L. D. Carr, D. DeMille, R. V. Krems, and J. Ye, New J. Phys. **11**, 055049 (2009).
[10] S. A. Moses, J. P. Covey, M. T. Miecnikowski, D. S. Jin, and J. Ye, Nat. Phys. **13**, 13 (2017).
[11] K. M. Jones, E. Tiesinga, P. D. Lett, and P. S. Julienne, Rev. Mod. Phys. **78**, 483 (2006).
[12] S. Ospelkaus, K.-K. Ni, D. Wang, M. H. G. de Miranda, B. Neyenhuis, G. Quéméner, P. S. Julienne, J. L. Bohn, D. S. Jin, and J. Ye, Science **327**, 853 (2010).
[13] K.-K. Ni, S. Ospelkaus, D. Wang, G. Quéméner, B. Neyenhuis, M. H. G. de Miranda, J. L. Bohn, J. Ye, and D. S. Jin, Nature (London) **464**, 1324 (2010).
[14] J. Pérez-Ríos, F. Herrera, and R. V. Krems, New J. Phys. **12**, 103007 (2010).
[15] A. Micheli, G. K. Brennen, and P. Zoller, Nat. Phys. **2**, 341 (2006).
[16] N. Nemitz, F. Baumer, F. Münchow, S. Tassy, and A. Görlitz, Phys. Rev. A **79**, 061403(R) (2009).
[17] J. D. Weinstein, R. deCarvalho, T. Guillet, B. Friedrich, and J. M. Doyle, Nature (London) **395**, 148 (1998).
[18] K. Maussang, D. Egorov, J. S. Helton, S. V. Nguyen, and J. M. Doyle, Phys. Rev. Lett. **94**, 123002 (2005).
[19] E. S. Shuman, J. F. Barry, D. R. Glenn, and D. DeMille, Phys. Rev. Lett. **103**, 223001 (2009).
[20] R. Krems, B. Friedrich, and W. C. Stwalley, *Cold Molecules: Theory, Experiment, Applications* (CRC Press, Boca Raton, 2009).
[21] P. S. Żuchowski, J. Aldegunde, and J. M. Hutson, Phys. Rev. Lett. **105**, 153201 (2010).
[22] D. A. Brue and J. M. Hutson, Phys. Rev. Lett. **108**, 043201 (2012).
[23] R. H. G. Reid and A. Dalgarno, Phys. Rev. Lett. **22**, 1029 (1969).
[24] M. L. González-Martínez and J. M. Hutson, Phys. Rev. A **88**, 020701(R) (2013).
[25] A. Petrov, C. Makrides, and S. Kotochigova, New J. Phys. **17**, 045010 (2015).
[26] T. Chen, C. Zhang, X. Li, J. Qian, and Y. Wang, New J. Phys. **17**, 103036 (2015).
[27] W. Dowd, R. J. Roy, R. K. Shrestha, A. Petrov, C. Makrides, S. Kotochigova, and S. Gupta, New J. Phys. **17**, 055007 (2015).
[28] H. Konishi, F. Schäfer, S. Ueda, and Y. Takahashi, New J. Phys. **18**, 103009 (2016).
[29] F. Schäfer, H. Konishi, A. Bouscal, T. Yagami, and Y. Takahashi, New J. Phys (2017), arXiv:1705.6841.
[30] H. Hara, Y. Takasu, Y. Yamaoka, J. M. Doyle, and Y. Takahashi, Phys. Rev. Lett. **106**, 205304 (2011).
[31] S. Kato, K. Inaba, S. Sugawa, K. Shibata, R. Yamamoto, M. Yamashita, and Y. Takahashi, Nat. Commun. **7**, 11341 (2016).
[32] S. Uetake, R. Murakami, J. M. Doyle, and Y. Takahashi, Phys. Rev. A **86**, 032712 (2012).
[33] C. H. Schunck, M. W. Zwierlein, C. A. Stan, S. M. F. Raupach, W. Ketterle, A. Simoni, E. Tiesinga, C. J. Williams, and P. S. Julienne, Phys. Rev. A **71**, 045601 (2005).
[34] V. V. Ivanov, A. Khramov, A. H. Hansen, W. H. Dowd, F. Münchow, A. O. Jamison, and S. Gupta, Phys. Rev. Lett. **106**, 153201 (2011).
[35] R. Roy, A. Green, R. Bowler, and S. Gupta, Phys. Rev. Lett. **118**, 055301 (2017).
[36] Z. Idziaszek and P. S. Julienne, Phys. Rev. Lett. **104**, 113202 (2010).